

A novel calculation strategy for optimized prediction of the reduction of electrochemical window at anode

Guochen Sun(孙国宸), Jian Gao(高健), and Hong Li(李泓)
Citation: Chin. Phys. B, 2023, 32 (**7**): 078201. DOI: 10.1088/1674-1056/accd51
Journal homepage: http://cpb.iphy.ac.cn; http://iopscience.iop.org/cpb

What follows is a list of articles you may be interested in

Structural, electronic, and Li-ion mobility properties of garnet-type $Li_7La_3Zr_2O_{12}$ surface: An insight from first-principles calculations

Jing-Xuan Wang(王靖轩), Bao-Zhen Sun(孙宝珍), Mei Li(李梅), Mu-Sheng Wu(吴木生), and Bo Xu(徐波)
Chin. Phys. B, 2023, 32 (**6**): 068201. DOI: 10.1088/1674-1056/acc05d

Computational screening of doping schemes for $LiTi_2(PO_4)_3$ as cathode coating materials

Yu-Qi Wang(王宇琦), Xiao-Rui Sun(孙晓瑞), Rui-Juan Xiao(肖睿娟), Li-Quan Chen(陈立泉)
Chin. Phys. B, 2020, 29 (**3**): 038202. DOI: 10.1088/1674-1056/ab7186

Tuning hybrid liquid/solid electrolytes by lowering Li salt concentration for lithium batteries

Wei Yang(杨伟), Qi-Di Wang(王启迪), Yu Lei(雷宇), Zi-Pei Wan(万子裴), Lei Qin(秦磊), Wei Yu(余唯), Ru-Liang Liu(刘如亮), Deng-Yun Zhai(翟登云), Hong Li(李泓), Bao-Hua Li(李宝华), Fei-Yu Kang(康飞宇)
Chin. Phys. B, 2018, 27 (**6**): 068201. DOI: 10.1088/1674-1056/27/6/068201

Redox-assisted Li^+-storage in lithium-ion batteries

Qizhao Huang(黄启昭) and Qing Wang(王庆)
Chin. Phys. B, 2016, 25 (**1**): 018213. DOI: 10.1088/1674-1056/25/1/018213

High-throughput theoretical design of lithium battery materials

Shi-Gang Ling(凌仕刚), Jian Gao(高健), Rui-Juan Xiao(肖睿娟), Li-Quan Chen(陈立泉)
Chin. Phys. B, 2016, 25 (**1**): 018208. DOI: 10.1088/1674-1056/25/1/018208

RAPID COMMUNICATION

A novel calculation strategy for optimized prediction of the reduction of electrochemical window at anode

Guochen Sun(孙国宸)[1,2], Jian Gao(高健)[3,†], and Hong Li(李泓)[1,‡]

[1] *Key Laboratory for Renewable Energy, Beijing Key Laboratory for New Energy Materials and Devices, Institute of Physics, Chinese Academy of Sciences, Beijing* 100190, *China*

[2] *College of Materials Sciences and Opto-Electronic Technology, University of Chinese Academy of Sciences, Beijing* 100049, *China*

[3] *College of Chemical Engineering, Beijing University of Chemical Technology, Beijing* 100029, *China*

(Received 20 March 2023; revised manuscript received 13 April 2023; accepted manuscript online 16 April 2023)

The reduction of the electrochemical window (EW) of electrolytes plays a significant role in assessing their compatibility with the anode in lithium-ion batteries. However, the accurate calculation of the reduction of EW is still challenging due to missing the solvation effects, condensation effects, kinetic factors, and the passivation on anodes. The theoretical prediction of the intrinsic and apparent EW is confirmed by a comprehensive experimental analysis of ethylene carbonate-dimethyl carbonate (EC-DMC) electrolytes, combining linear sweep voltammetry (LSV) and gas chromatography-mass spectrometry (GC-MS). The proposed novel kinetic normal distribution theory model can quantitatively explain the current density from LSV and affirm acetaldehyde (MeCHO) as one of the primary reduction products of EC. The solvent effect restricts the intrinsic EW of EC-DMC without lithium salt to 2.6 V (vs. Li^+/Li) arising from the Marcus–Gerischer theory and the passivation of MeCHO on the anode broadens the apparent EW to 0.3 V (vs. Li^+/Li) arising from the normal distribution of the lowest unoccupied molecular orbital (LUMO) for MeCHO produced by thermal motion. In addition, the passivation on the anode depends intensively on the lithium salt, resulting in more complicated influences on the apparent EW.

Keywords: lithium battery, electrolyte, reduction kinetic, electrochemical window

PACS: 82.47.Aa, 82.45.Gj, 65.40.gk, 87.15.R– **DOI:** 10.1088/1674-1056/accd51

1. Introduction

Extending lithium-ion battery life is a priority for the development of electric vehicle power batteries, energy storage batteries, recycling technology, and reducing the environmental pollution.[1] Efforts are carrying out on altering electrolytes, adding additives, and performing high-throughput calculations to screen new systems,[2] as well as developing the predictive models of battery life based on impedance and failure analysis to understand the inner mechanism of capacity fading.[3,4] Having been widely recognized, the continuous growth of thickened solid electrolyte interphase (SEI) on the anode primarily accounts for the decay of capacity for commercial battery systems, which comes from the decomposition of electrolytes and consuming lithium ions.[5,6] However, the electrolyte, which can be compatible with the anodes with lower electric potential, is still urgently demanded, in order to increase the energy density. For example, several common solvents, such as propylene carbonate (PC) and dimethyl ether (DME), fail to accommodate the most popular graphite anode, which further limits the options for the solvent.[7] The complex side reaction on anodes brings difficulties in the comprehension of the decomposition mechanism and reaction conditions. However, it is essential to accurately predict electrolytes' stability and compatibility with the lower electrical potential anodes for rational selection and design of the electrolyte systems for long-life battery systems.

Extensive experimental methods are applied to focus on various aspects. Aiming at the observation of SEI films with thickness ranging from a few nanometers to tens of nanometers, the recently developed cryogenic transmission electron microscopy (cryo-TEM) succeeds in observing with slight damage. On the same carbon black anode, both 5 nm and 100 nm SEI can be observed due to the highly heterogeneous process influenced by multiple factors of SEI growth.[8] Also due to the complicated decomposition reactions, graphite layers are observed to be peeled off in graphite ethylene carbonate-diethyl carbonate (EC-DEC), which is generally thought to occur only in PC.[9] Focusing on the complex decomposition products and reaction pathways, the combination of nuclear resonance spectroscopy (NMR), gas chromatography-mass spectrometry (GC-MS), attenuated total reflectance infrared spectroscopy (ATR-IR), and x-ray photoelectron spectroscopy (XPS) is applied.[10] The electron paramagnetic resonance (EPR) spectroscopy confirms that the reduction pathway is influenced strongly by external energy,[11] and the operando neutron reflectometry and quartz

†Corresponding author. E-mail: gaojian@mail.buct.edu.cn

‡Corresponding author. E-mail: hli@iphy.ac.cn

© 2023 Chinese Physical Society and IOP Publishing Ltd

crystal microbalance methods help to distinguish the potential of growth inner and outer layers of SEI under different electrode potentials.[12] The gas chromatography combined with mass spectrometry can distinguish the sole characteristic of ion fragments for verifying the species of substances and help to detect the trace content and concentration of products in the electrolytes.[13]

The initial reduction processes of EC have been theoretically investigated extensively,[14–23] and several pathways are proposed for the specific decomposition of EC, among which the dominant one is decided by the competing reaction rates and electrode potentials during each process. However, the theoretical quantification of the reduction of the electrochemical window is still challenging. Previously, the reduction of EW is usually calculated as the electronic affinity (EA) between the neutral molecule and the reduced molecule with negative valence.[24] However, the electric potential of EA is relative to the equilibrium potential (φ^0) formed by the calculated two structures before and after charging, i.e., $\mathrm{EA} = F(\varphi - \varphi^0)$, ($F$ is the Faraday constant), according to the Butler–Volmer theory.[25,26] And different electric pairs generally have different φ^0s, which will bring in errors when directly comparing the EA between different materials.[26] The equilibrium potential of lithium-ion dissolved in solvent relative to lithium metal calculated from dissolving free energy is also proposed as an approximation to represent EW.[27] Another approach is to obtain the surface potential at zero charge by calculating the linear relationship between the surficial potential and the surface electron density from a series of charged models. Then when the surficial charge density is extrapolated to zero, the simulated surficial potential can be regarded as the conservative electrochemical window, because neither net in nor out flux of charged carriers (ions and electrons) across the balanced interface between the electrode and the electrolyte under the above zero charge potential condition.[28] After a long period of confusion, recently, an improved thermodynamic cycle method is proposed, involving crucial reorganization energy and solvation energy in predicting EW, then the mean-absolute-errors can be decreased from 3.25 V by the traditional method to 0.68 V after corrections, revealing the source of the dominant errors.[29] In addition, the solvent effect is also pivotal in the study of the redox kinetics of interfacial reactions in the Li-air battery.[30] Besides all the above corrections, the improvement of the accuracy in predicting EW is still in demand, and the only test standard should be account for the actual battery performance.

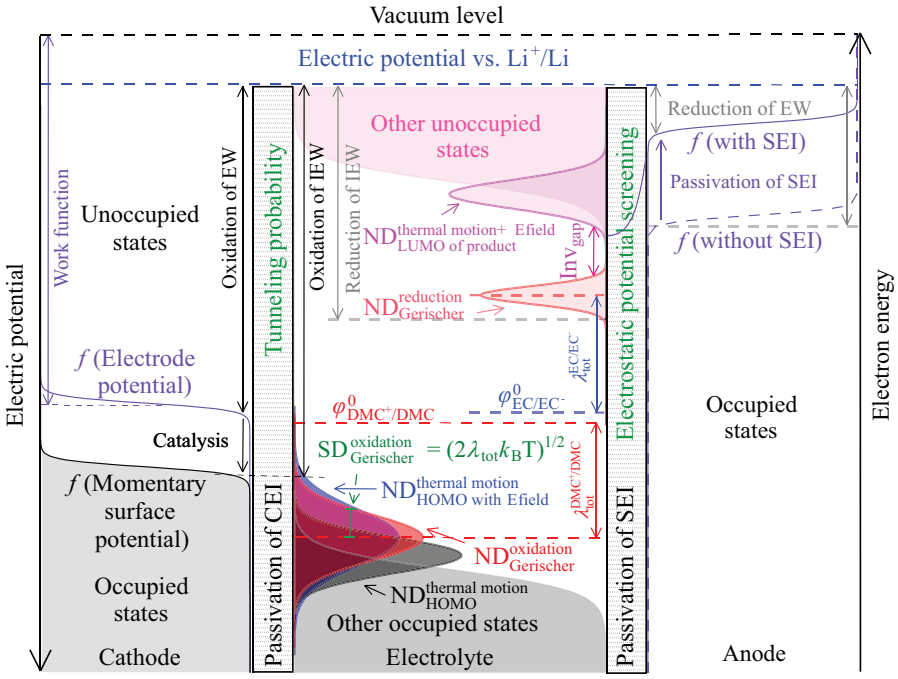


Fig. 1. The schematic relationship between electronic states of cathode, anode, and the normal distribution of Gerischer model, the HOMO of electrolytes, the LUMO of decomposition product, and electrochemical window. EW, IEW, ND, SD, SEI, CEI, E_{field}, f, λ_{tot}, $\varphi^0_{\mathrm{Ox/Red}}$ respectively represent the electrochemical window, intrinsic electrochemical window, normal distribution for condensed phase solution, standard deviation, solid electrolyte interphase, cathode-electrolyte interphase, interfacial electric field, Fermi distribution, total reorganization energies, and equilibrium potential of the redox couple.

This study is focused on analyzing the complicated electrochemical characteristic of *in situ* linear sweep voltammetry (LSV) curves for solvents and the influence of corresponding passivation products on EW. A novel model based on thermodynamics and kinetics of electrochemical reduction with the Marcus–Gerischer solvent effect theory, the amendment of the lowest unoccupied molecular orbital (LUMO) based on the effects of condensation, thermal motion, and the interfacial electric field is proposed, which is in good consistent with the LSV curves and EWs. The *in situ* electrochemical signal

LSV is applied to reveal the complex electrochemical characteristics which arise from the complicated passivation at the anode, and the intrinsic thermodynamic and kinetic properties of EC. By the combined analysis of calculation, LSV, and GC-MS, the decomposition product is detected, and its influence on the electrochemical process is discussed. With the correction of the passivation effect observed from experiments, the LSV and reduction of EW in different passivation cases are explained by the proposed novel kinetic model, as summarized in Fig. 1. Details of experiment and calculation method are provided in the supplementary information.[31–46]

2. Results and discussion

2.1. Intrinsic reduction electrochemical window of EC

Firstly, the LSVs of EC-DMC (1:1 vol%) start from the φ^0 towards negative electric potential until −0.2 V with and without rotating disk electrode (RDE) are measured as shown by the red and green curves in Fig. 2(a). Tetrabutylammonium p-toluenesulfonate (TBATOS) is chosen as the supporting electrolyte instead of other salts,[47] for its stability within the measurement range (Fig. S1), which extends the low potential to −0.2 V vs. Li^+/Li. When measured with a glassy carbon working electrode without RDE, a tiny peak appears at 2.35 V, which is easy to be ignored in comparison to the large absolute current density around 0 V. The absolute current increases when the electric potential is decreased to 2.35 V with an RDE of 2000 rpm, indicating the appearance of a reduction reaction of some components. Different from the conventional method, RDE eliminates diffusion, promotes the transfer of reactant, and cleans away the passivation of the product, which facilitates distinguishing the intrinsic electrochemical characteristics of the solvent. Therefore, EC and DMC are measured separately to further identify the reduction current in Fig. 2(b), holding all the measurement conditions as Fig. 2(a), but increasing the temperature to 60 °C for melting EC. The measurements of DMC in Fig. 2(b) and EC-DMC in Fig. 2(a) under 60 °C are also provided, and the temperature is controlled to the same variable to exclude its influence on the reduction mechanisms for current density, for each curve has the same shape but increased current density from 25 °C to 60 °C. When the RDE is applied and the potential is decreased to 2.35 V, both the absolute currents increase for EC and DMC. However, the shapes of LSVs with RDE respective EC and DMC are different.

Comparing the LSV shapes of EC-DMC, EC, and DMC with RDE, the reduction current for EC around 2.35 V dominates the reduction of the mixed EC-DMC system, which could be explained by the Marcus–Gerischer theory: a coordinated molecular or ion stabilized by the coordinated solvent molecules with the comprehensive interaction, including the Coulomb attraction and multi-weak interaction, steric effects, collectively referred to as "the solvent effect in the Marcus theory", i.e., the "solvent effect", and it will bring the positions of the stable structures for oxidation and reduction close to each other on the potential energy surface (PES), and build a pathway for electrochemical redox. The reduction from the solvent effect weakens the intrinsic stability of the electrolyte, owing to the reduction potential of the solvent effect at the inside of the apparent EW of the EC-DMC electrolyte at 0.3 V in Fig. 2(a). This solvent effect explains the kinetic reduction of the electrolytes by searching stable solvent clusters, combining hybrid explicit and implicit solvent models, and applying the kinetics normal distribution models, shown as the process searching the lowest total reorganization energy (λ_{tot}) in supplementary information. Therefore, the absolute reduction currents $R(U)$ of RDE around 2.35 V could be solved by a kinetic electrochemical model, including the Gerischer model, which is integrated with a normal distribution of the electronic state $\varphi(U_{Li}, SD)$ for EC,

$$R(U) = \frac{1}{\Delta t} S d N_A C_{bulk} \int_{-\infty}^{\infty} f(U_{Li}, U)\, \varphi(U_{Li}, \sigma)\, dU_{Li}, \quad (1)$$

where $f(U_{Li}, U)$ is the Fermi distribution, Δt the measuring unit time, S the contact area, d the average distance of transportation of electrons, N_A the Avogadro constant, and C_{bulk} the bulk concentration of quasi-oxidation molecules.

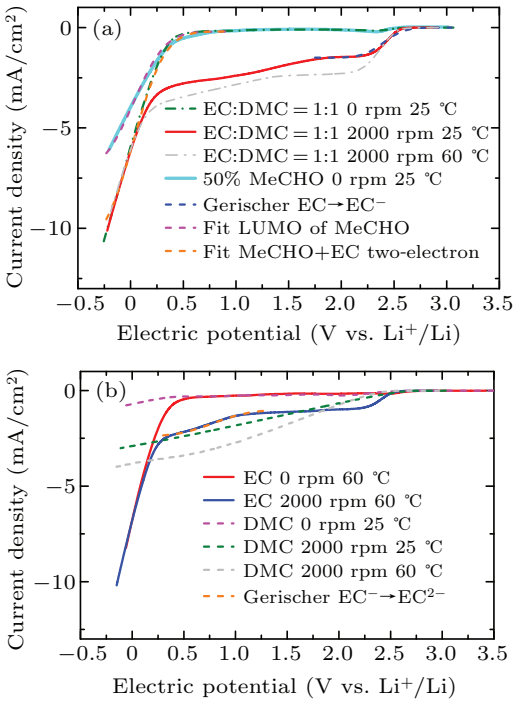


Fig. 2. LSV measured by a rotating disk electrode (RDE) with a glassy carbon working electrode at 25 °C and 60 °C. (a) Experimental LSVs in solid curves: ethylene carbonate-dimethyl carbonate (EC-DMC 1:1 vol%) mixed electrolytes or acetaldehyde (MeCHO) both with tetrabutylammonium p-toluenesulfonate (TBATOS) as supporting electrolytes. Calculational LSVs in dashed curves: from the solvent effect of the Marcus–Gerischer model and the broadened distribution of LUMO for MeCHO by thermal motion and interfacial electric field. (b) Experimental LSVs for EC and DMC measured respectively with and without RDE.

The average electronic state distribution of solvent effect from the Gerischer model for EC equals 2.35 V and the standard deviation (SD, σ) is 0.15 V, drawn as the dark blue dashed curve in Fig. 2(a) by our extended model. The intrinsic EW of EC-DMC is also restricted by the solvent effect equaling $\overline{\mathrm{ND}}_{\mathrm{Gerischer}} + \frac{\sqrt{2\pi}}{2}\mathrm{SD}_{\mathrm{Gerischer}} = 2.6$ V (details in the supplementary information). Whereas the reduction of DMC with RDE has a linear current relative to overpotential like a capacitance, which could be derived from the more stable bonds in DMC than EC, thus the DMC decomposition is depressed, and the further molecules reduction is also depressed by the covering of firm ion clusters of reduced DMC due to the Coulomb interaction.

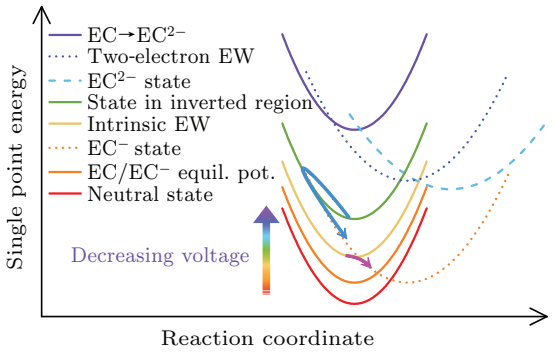


Fig. 3. A schematic of the potential energy surface (PES) for neutral, charged-1, and charged-2 states of EC during reduction according to the Bulter–Volmer model and the Marcus theory.

Deduced from the Marcus theory, the growth rate of EC reduction is depressed within the range between 1.75 V and 2.35 V in Figs. 2(a) and 2(b), called the inverted region (Fig. 3), which is derived from the gap in the inverted region ($\mathrm{Inv}_{\mathrm{gap}}$ in Fig. 1) between the reduction of normal distribution of the Gerischer model ($\mathrm{ND}^{\mathrm{reduction}}_{\mathrm{Gerischer}}$) and the reduction of normal distribution of thermal motion ($\mathrm{ND}^{\mathrm{thermal\ motion}}_{\mathrm{LUMO}}$) of the product. Because the electronic state of electrolytes breaks in the $\mathrm{Inv}_{\mathrm{gap}}$, the current density of RDE in the inverted region will not increase, and the reduction current totally comes from the $\mathrm{ND}^{\mathrm{reduction}}_{\mathrm{Gerischer}}$. Another deduction of the inverted region is the max current density without RDE presented at 2.35 V, equaling the φ^0 minus λ_{tot}/e, and the energy barrier of the transition state $\Delta G_{\mathrm{f}}^{\neq} = \frac{\lambda_{\mathrm{tot}}}{4}(1 + \frac{F(\varphi-\varphi^0)}{\lambda_{\mathrm{tot}}})^2$ doesn't fall but increases when the electric potential decreases below $\varphi^0 - \lambda_{\mathrm{tot}}/e$, even though the variation of the reaction free energy decreases monotonously. Meanwhile, from the PES perspective, the point of intersection for neutral and charged PES is higher than the energy of the initial stable state in the inverted region, and the redox progress should move on the neutral PES and reach the intersection point before getting or losing the electron moving to the charged PES as the blue arrow in Fig. 3. Therefore, the calculation of the decomposition process, such as the breakage of bonds, in the inverted region should search from the neutral PES priorly rather than modeling with a charged state, such as directly setting the system with an extra initial charge. Since most quantum chemistry programs cannot continuously simulate the external potential, the subsequent study of the product is simplified to the state of the whole charge number.

2.2. Reduction products of EC around intrinsic reduction electrochemical window

Acetaldehyde (MeCHO) is the foremost reduction product during decreasing the electric potential, which is confirmed from the searching by the relaxed scan calculations of the bond energies for each bond in EC on the neutral state (supplementary information), also detected by the GC-MS when electrolysis at 1.75 V (Table 1 and Fig. 4). The maximum concentration of MeCHO detected by GC-MS presents at 1.75 V, indicating MeCHO is the reduction product from the Marcus–Gerischer theory (Table 1), written as

$$\mathrm{EC} + \mathrm{e}^- \xrightarrow{\text{solvent effect}} \mathrm{CO_2} + \mathrm{CH_3CHO^-}. \tag{2}$$

Revealed by GC-MS, the concentration of MeCHO increased from 6.2 nmol/mL to 47 nmol/mL five days later after electrolysis, consistent with the Marcus mechanism that EC reduction in the inverted region is motivated by additional electrons or ions, following the neutral PES preferentially, written as

$$\mathrm{EC} + \mathrm{CH_3CHO^-} \xrightarrow{\text{in solvent}} \mathrm{CO_2} + \mathrm{CH_3CHO} + \mathrm{CH_3CHO}. \tag{3}$$

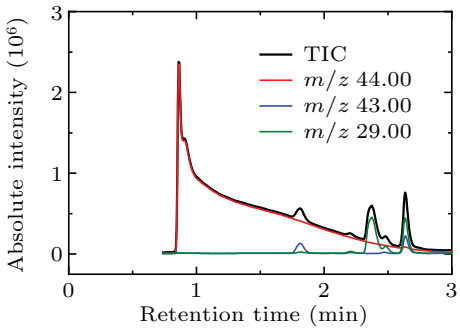


Fig. 4. "Liquid" GC-MS chromatograms of electrolyzed EC-DMC at 1.75 V vs. $\mathrm{Li^+/Li}$ and the detected production of acetaldehyde with three characteristic m/z of 44, 43, and 29 and the total ion chromatography (TIC).

The product MeCHO originates from the lack of lithium-ion involvement and appears only at relatively high potentials, in contrast to those reported mechanisms that require the consumption of lithium ions or only at low potentials where EC decomposes by two-electron reduction.[25] The one-electron reduction process is possible due to that the uncoordinated solvent molecules are higher than the coordinated one in 1 mol/L $\mathrm{LiPF_6}$ with EC-DMC (1:1 vol%), which has the molar ratio between lithium-ion and solvent of around 1:13 and the coordinated number between solvent and $\mathrm{Li^+}$ of about 4. And when the lithium-ion concentration is insufficiency restricted by diffusion, formula (2) could be a main decomposition pathway at high electrode potential, because, with the passivation

of SEI, the surface potential on SEI will rise much higher than the anode preventing electrolytes decomposed continuously at low electrode potential.

Table 1. Concentration of acetaldehyde (nmol/mL) ($m/z = 44$) by constant potential electrolysis of EC-DMC (1:1 vol%) for glass carbon (GC) and graphite at different electric potentials.

Working electrode	0 V	0.35 V	1.75 V	2.5 V
GC 5 min	16.5	34.5	97.8	22.9
GC 1 min	5.2	5.6	6.2	5.1
GC 1 min 5 days later	14	16	47	13
Graphite 5 min	11.9	13.8	24.8	20.9
Graphite 1 min	5.5	5.8	8.0	6.8

2.3. Sections of reduction LSV

Furthermore, the LSV of EC-DMC with RDE could be separated into four sections (in Fig. 2): firstly, from 2.5 V to 1.5 V, reduction current restrained by the solvent effect, and 2.35 V is the intrinsic EW of EC-DMC as clarified above. From 1.5 V to 1.0 V, the reduction of DMC participates in the reduction current, which is identified from the LSV of DMC in Fig. 2(b). From 1.0 V to 0.3 V, EC^- reduced to EC^{2-} by the solvent effect of the Marcus–Gerischer theory, fitted as the orange dashed curve in Fig. 2(b), which is deduced from the consistency of experimental and calculated current density. However, in the same electric potential range (1.0–0.3 V) of EC-DMC, the growth rate of current density for EC-DMC with RDE (red curve in Fig. 2(a)) is decreased rather than increased, which might be influenced by the Coulomb repulsive interaction of charged ions on the interface, where the coordinated solvent structure prevents the further reduction and decreases the mobility.

Under 0.3 V, the absolute current density of each system containing EC increases rapidly and reaches 10 mA/cm^2 at −0.2 V. Such intensive and sharp current density could only result from the direct reduction of LUMO inferred from our kinetic model. Furthermore, it should be attributed to the decomposed product, which has a larger C_{bulk} in formula (1), indicating smaller molecular volume than EC, leading to the experimental current density markedly larger than the theoretical one. The calculation of the LUMO of EC also supports this conclusion (Fig. 5(a)): the average normal distribution of LUMO ($ND_{LUMO}^{thermalmotion}$) for EC-DMC equals −1.38 V vs. Li^+/Li. Both quantum chemistry (QC) extrapolated to a macroscopical solution (Fig. 5(b)) and *ab initio* period calculation, which aligned the absolute position of the density of states (DOS) to QC, conclude in consistent band gaps (Fig. 5(a)) for both PBE and B3LYP functional, confirming the accuracy of ND. The UV-vis absorption spectrum dominated by the highest occupied molecular orbital HOMO–LUMO excitation also proves the position of LUMO no more than −0.45 V (Fig. S3). Therefore, the reduction current below 0.3 V in Fig. 2 is not derived from the LUMO of EC.

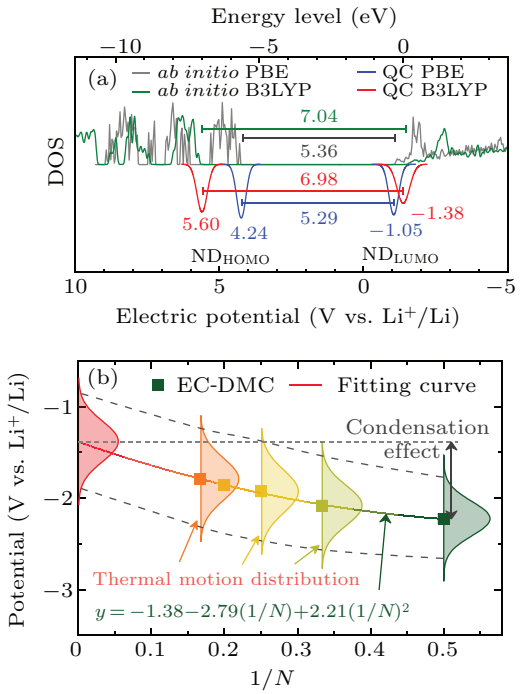


Fig. 5. (a) Normal distributions (ND) of HOMO and LUMO for EC-DMC (1:1) under thermal motion by AIMD, the statistics of quantum chemistry (QC) single point calculations, and extrapolating the number of molecules to infinite, comparing with the density of state (DOS) from *ab initio* period calculation with PBE and B3LYP functional. (b) The relationship between the normal distribution of thermal motion for LUMO and the number of molecule pairs (N) of EC-DMC by QC with B3LYP functional.

2.4. Origin of apparent electrochemical window for EC

MeCHO is one of the decomposition products for EC, as mentioned above, and the LSV simulated from the normal distribution of LUMO (ND_{LUMO}) for MeCHO (pink curve in Fig. 2(a)), which is below 0.3 V, agrees with the experimental LSV of MeCHO (azury curve in Fig. 2(a)). There is a gap between the experimental current density of EC-DMC and MeCHO, and the latter is divided by 2 to suit the concentration of MeCHO the same as the concentration of EC in EC-DMC (1:1 vol%). Appending the two-electron reduction mechanism of EC to the simulated LSV of MeCHO, the fitting curve agrees with the experimental one, indicating the reduced product MeCHO could form unstable passivation on the interface of glass carbon (GC) electrode, thus preventing the further reduction of solvents at high electric potential; when the electric potential is decreased to lower than ND_{LUMO}, MeCHO decomposes rapidly and impairs the protection for EC, especially in the case of the LSV without RDE.

2.5. Reduction of EC-DMC on graphite anode

As the most common anode material in lithium batteries, graphite shows larger current density than GC, especially within the decomposition range between 1.2 V and 0.3 V (pink curve in Fig. 6(a)). The increased current density could mainly fit from the MeCHO reduction under RDE (azury curve in Fig. 6(a)), indicating the MeCHO passivation effect on the surface of GC or graphite is different. For graphite, the uneven edge and interspace between layers lead to a larger contact

area, which might break the unstable passivation by MeCHO and aggravate the MeCHO decomposition. Besides, the coincidence of experimental LSV under 1000 rpm RDE and the segmented calculation curves from the Gerischer model (red dashed curve in Fig. 6(a)) corrected by the ND_{LUMO} proves again the electrochemical reaction follows the most probable pathway for each feasible pathway.

2.6. Passivation effect of lithium salt

For the electrolytes with $LiPF_6$, the passivation layer is caused by the decomposition of $LiPF_6$ with solvent and contains highly robust products. Even with a high sweep speed of 50 mV/s, effective passivation occurs on the surface of GC after the first LSV, as depicted in Fig. 6(b), and the surficial electric potential on SEI is increased to higher than the EW of MeCHO. Further passivation with a low sweep speed of 1 mV/s can prevent the decomposition of EC-DMC until 0 V. Although the apparent EW does not have a unique standard that takes all kinds of passivation effects into consideration, the efforts on the analysis of the EW from solvent effect, LUMO, and the electrochemical characterization of the product can help in the selection and design of the electrolytes. As a result, SEI is a crucial phase in maintaining the performance of lithium batteries since the intrinsic EWs of most solvents are too narrow to match the low electric potential at the anodes of lithium-ion batteries.

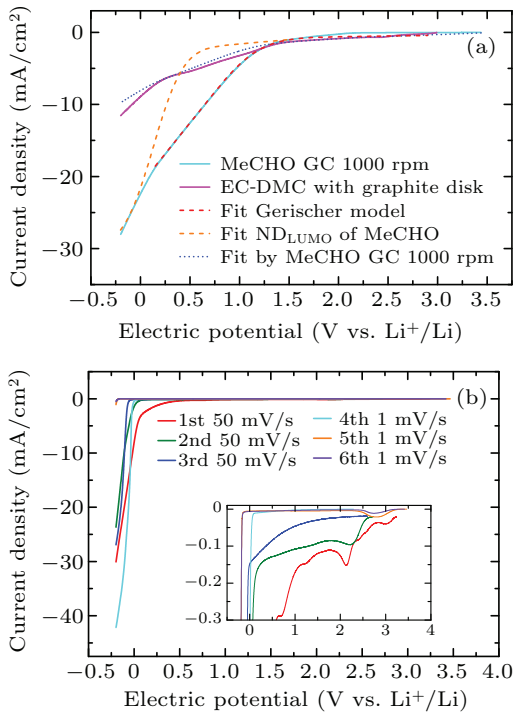


Fig. 6. (a) LSVs of acetaldehyde (MeCHO) with glassy carbon (GC) made RDE as working electrode, EC-DMC with a graphite disk as working electrode, calculated LSVs by the Gerischer model and the normal distribution of LUMO for MeCHO, and the fitting curve from the experimental LSV of MeCHO to the reduction of EC-DMC with a graphite disk working electrode. (b) LSVs of 1 mol/L $LiPF_6$ EC-DMC with GC working electrode.

2.7. Accuracy of the calculation model on other electrolytes

The apparent EW on the electrolyte reduction depends on the reduction products, such as SEI, rather than the electrolyte itself discussed previously.[48] As a result, it is of critical importance to identify these substances and discuss the role of each composition, which brings synergistic complexity. Furthermore, as an opposite example, the apparent EW of acrylonitrile is restricted by the LUMO of itself investigated as the accurate calculation model. Herein, the LSV is carried on with the glassy carbon as the working electrode (without RDE), and TBATOS as the supporting electrolyte, and a three-electrode system for acrylonitrile shown in Fig. 7. The reduction current lower than 1 V in Fig. 7(a) comes from the normal distribution of LUMO verified by the result calculated from formula (1), and the extrapolated ND_{LUMO} of acrylonitrile is shown in Fig. 7(b). One peak occurs at 2.4 V, corresponding to the reduction arising from the solvent effect, which is verified by the calculations (details in the supplementary information).

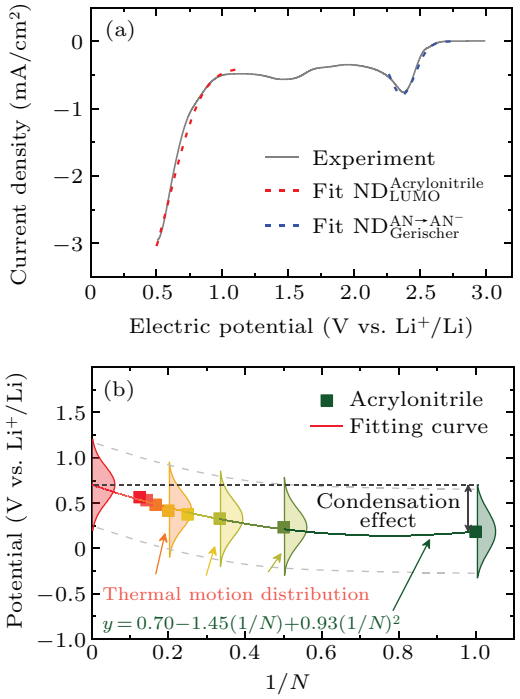


Fig. 7. (a) Experimental LSV for acrylonitrile measured with glassy carbon working electrode without RDE, and the corresponding calculated LSVs from the normal distribution of LUMO corrected by thermal motion and interfacial electric field, and the normal distribution of the solvent effect of the Gerischer model. (b) The relationship between the normal distribution of thermal motion for LUMO of acrylonitrile under thermal motion and the reciprocal of the number of model molecules (N) by QC with B3LYP functional.

3. Conclusion

The intrinsic EW of EC is 2.6 V derived from the solvent effect of the Marcus–Gerischer model, and the calculated results are confirmed by the LSV with RDE. In the situation

without the participation of lithium ions, acetaldehyde is the primary one-electron reduction product of EC. In comparison, in the more common and actual situations with existing diffusion control, i.e., where the RDE is not applied and the diffusion process is non-negligible, the physical adsorption of acetaldehyde and electrostatic adhesion of acetaldehyde ion lead to the passivation effect at the glassy carbon working electrode, leading to resist reactant in outer layers further access the interface. As a result, the absolute current density is reduced, and the apparent EW of the EC-DMC electrolyte is broadened up to 0.3 V. However, as the adsorption or adhesion of MeCHO can break away during a charge–discharge process and dissolution, this passivation effect is unstable. In addition, the restricted apparent EW is caused by the ND_{LUMO} of thermal motion arising from acetaldehyde rather than EC or DMC. Therefore, the successful application of EC-DMC with $LiPF_6$ is primarily attributed to the rigid passivation of SEI arising from the decomposition product of electrolytes, especially the lithium salt therein. And the increasing surficial electric potential by SEI facilitates alleviating the decomposition of the electrolytes.

Deducted from the theory model, SEI with a thickness of the order of a few nanometers is enough to prevent solvent decomposition caused by electric potential, due to the average distance of transportation of electrons d in formula (1) is only as small as the thickness of one single layer of molecules and the overpotential decays rapidly whatever in SEI or electrolyte according to the elaboration of the distribution of the electrostatic potential in the Helmholtz layer by the double-layer theory. However, the thickness of SEI larger than 100 nm is still reported in some experimental research. Acetaldehyde is identified as one of the unstable decomposition products of EC, and this reaction mechanism is revealed in this study. It is a pivotal factor to limit the battery life because of the narrow initial intrinsic EW of reduction as 2.6 V. Partial constituents in SEI are inevitably unstable, and the dynamical dissolution and growth of SEI hold on during the cycling of batteries until the electrolytes are dried and the batteries fail. Moreover, acetaldehyde is easy to react with lithium metal and leads to hydrogen gas, which leads to continuous SEI growth and potential insecurity. In conclusion, this study proposes that the detailed analysis of the successive physical and electrochemical processes as well as the corresponding products is critical to evaluate the compatibility of an electrolyte with the specific anode. Other details, for example, the process such as the embedding of solvent in graphite and solvent solvated-structure need to be considered to design the electrolytes systemically. This study also elaborately proposes a combined novel electrochemical kinetic model which takes the solvent effect from the free energy perspective and the amended distribution of energy level by thermal motion and electric field in consideration, disassembling the LSV curve shape to different reaction mechanisms. Further investigations are still in demand for the more nuanced decomposition products and mechanism of electrolytes, and further information can be applied for a more accurate prediction of the stability of electrolytes and the compatibility with anode.

Acknowledgements

Project supported by the National Natural Science Foundation of China (Grant Nos. U1964205 and 22109005), the National Key Research and Development Program of China (Grant No. 2016YFB0100100), and Beijing Municipal Science & Technology Commission, China (Grant No. Z191100004719001).

References

[1] Harper G, Sommerville R, Kendrick E, *et al.* 2019 *Nature* **575** 75
[2] Xu K 2014 *Chem. Rev.* **114** 11503
[3] Severson K A, Attia P M, Jin N, *et al.* 2019 *Nature Energy* **4** 383
[4] Qiao R X, Zhang M J, Liu Y D, *et al.* 2016 *Chin. Phys. Lett.* **33** 078201
[5] Liu W, Liu P and Mitlin D 2020 *Advanced Energy Materials* **10** 2002297
[6] Hou C, Han J, Liu P, *et al.* 2019 *Advanced Energy Materials* **9** 1902675
[7] Xu K 2004 *Chem. Rev.* **104** 4303
[8] Huang W, Attia P M, Wang H, *et al.* 2019 *Nano Lett.* **19** 5140
[9] Han B, Zou Y, Xu G, *et al.* 2021 *Energy Environ. Sci.* **14** 4882
[10] Parimalam B S, Macintosh A D, Kadam R, *et al.* 2017 *The Journal of Physical Chemistry C* **121** 22733
[11] Shkrob I A, Zhu Y, Marin T W, *et al.* 2013 *The Journal of Physical Chemistry C* **117** 19255
[12] Lee C H, Dura J A, Lebar A, *et al.* 2019 *Journal of Power Sources* **412** 725
[13] Gachot G, Ribiere P, Mathiron D, *et al.* 2011 *Anal. Chem.* **83** 478
[14] Ganesh P, Kent P R C and Jiang D E 2012 *The Journal of Physical Chemistry C* **116** 24476
[15] Ushirogata K, Sodeyama K, Okuno Y, *et al.* 2013 *J. Am. Chem. Soc.* **135** 11967
[16] Tasaki K 2005 *J. Phys. Chem. B* **109** 2920
[17] Leung K 2013 *Chem. Phys. Lett.* **568–569** 1
[18] Spotte-Smith E W C, Kam R L, Barter D, *et al.* 2022 *ACS Energy Letters* **7** 1446
[19] Hossain M J, Pawar G, Liaw B, *et al.* 2020 *J. Chem. Phys.* **152** 184301
[20] Martinez De La Hoz J M, Leung K and Balbuena P B 2013 *ACS Appl. Mater. Interfaces* **5** 13457
[21] Liu Y, Wu Y, Sun Q, *et al.* 2022 *Adv. Theory Simul.* **5** 2100612
[22] Ebadi M, Brandell D and Araujo C M 2016 *J. Chem. Phys.* **145** 204701
[23] Ohba N, Ogata S and Asahi R 2019 *The Journal of Physical Chemistry C* **123** 9673
[24] Borodin O 2019 *Current Opinion in Electrochemistry* **13** 86
[25] Wang A, Kadam S, Li H, *et al.* 2018 *npj Computational Materials* **4** 15
[26] Bard A J and Faulkner L R 2000 *Electrochemical Methods: Fundamentals and Applications*, 2nd Ed. (New York: John Wiley & Sons, Incorporated.) pp. 115–132
[27] Wang Y, Nakamura S, Ue M, *et al.* 2001 *J. Am. Chem. Soc.* **123** 11708
[28] Leung K and Tenney C M 2013 *The Journal of Physical Chemistry C* **117** 24224
[29] Wang D, He T, Wang A, *et al.* 2023 *Advanced Functional Materials* **33** 2212342
[30] Wang A, Zou Z, Wang D, *et al.* 2021 *Energy Storage Materials* **35** 595
[31] Stephens P J, Devlin F J, Chabalowski C F, *et al.* 1994 *The Journal of Physical Chemistry* **98** 11623
[32] Hehre W J, Ditchfield R and Pople J A 1972 *The Journal of Chemical Physics* **56** 2257

[33] Zade S S, Zamoshchik N and Bendikov M 2011 *Accounts of Chemical Research* **44** 14
[34] Manzetti S and Lu T 2013 *RSC Advances* **3** 25881
[35] Marcus R A 1956 *The Journal of Chemical Physics* **24** 966
[36] Marcus R A 1968 *Electrochimica Acta* **13** 995
[37] Pracht P, Bohle F and Grimme S 2020 *Phys. Chem. Chem. Phys.* **22** 7169
[38] Bannwarth C, Ehlert S and Grimme S 2019 *J. Chem. Theory Comput.* **15** 1652
[39] Grimme S 2019 *J. Chem. Theory Comput.* **15** 2847
[40] Bannwarth C, Caldeweyher E, Ehlert S, *et al.* 2020 *WIREs Comput Mol Sci.* **11** e1493
[41] Neese F 2018 *WIREs Comput Mol Sci.* **8** e1327
[42] Weigend F and Ahlrichs R 2005 *Phys. Chem. Chem. Phys.* **7** 3297
[43] Frisch M J, Trucks G W, Schlegel H B, *et al.* 2009 *Gaussian 09* Rev. D.01. Wallingford, CT
[44] Nelsen S F, Blackstock S C and Kim Y 1987 *Journal of the American Chemical Society* **109** 677
[45] Hoffmann J S, O'connor R T, Magne F C, *et al.* 1956 *J. Am. Oil Chem. Soc.* **33** 410
[46] Caldeweyher E, Bannwarth C and Grimme S 2017 *J. Chem. Phys.* **147** 034112
[47] Dziewonski P M and Grzeszczuk M 2010 *J. Phys. Chem. B* **114** 7158
[48] Winter M Barnett B and Xu K 2018 *Chem. Rev.* **118** 11433